Journal of Clinical and Translational Hepatology **2025**
DOI: 10.14218/JCTH.2025.00538

Original Article

Bidirectional Regulation between Metabolic Dysfunction-associated Steatotic Liver Disease and Sarcopenia via Liver-muscle Crosstalk

Yeyu Song[1,2], Yameng Liu[2], Jie Jiang[2], Youjie Zheng[3], Zixuan Wang[1], Cen Xie[2*] and Jian-Gao Fan[1,3*]

[1]Center for Fatty Liver, Department of Gastroenterology, Xinhua Hospital Affiliated to Shanghai Jiao Tong University School of Medicine, Shanghai, China; [2]State Key Laboratory of Drug Research, Shanghai Institute of Materia Medica, Chinese Academy of Sciences, Shanghai, China; [3]Shanghai Key Laboratory of Pediatric Gastroenterology and Nutrition, Shanghai, China

Received: October 14, 2025 | **Revised:** November 26, 2025 | **Accepted:** December 04, 2025 | **Published online:** January 07, 2026

Abstract

Background and Aims: Metabolic dysfunction-associated steatotic liver disease (MASLD) and sarcopenia frequently coexist, yet their causal relationship and underlying mechanisms remain poorly defined. This study aimed to investigate whether a bidirectional causal link exists between MASLD and sarcopenia and to identify the molecular mediators involved in liver-muscle crosstalk. ***Methods:*** We applied Mendelian randomization to test the causal effect of sarcopenia-related traits on MASLD risk. To capture distinct clinical features, we established complementary mouse models, including diet-induced and genetic (*ob*/*ob*) MASLD models, a stelic animal model, and a drug-induced muscle atrophy model. Multi-tissue transcriptomic profiling was performed on liver and muscle to uncover altered pathways. ***Results:*** Complementing prior genetic evidence establishing MASLD as a causal factor for sarcopenia, our Mendelian randomization analysis revealed that diminished muscle mass and muscle function contribute to an elevated risk of MASLD. In mice with MASLD, we observed loss of muscle mass, reduced strength, and ectopic lipid deposition in skeletal muscle. Conversely, muscle atrophy exacerbated hepatic steatosis, inflammation, and fibrosis in MASLD mice. Transcriptional profiling revealed that sarcopenia impairs hepatic metabolic homeostasis by enhancing fatty acid uptake and impairing oxidative phosphorylation, while MASLD, in turn, promotes muscle dysfunction by exacerbating inflammatory responses and metabolic dysfunction. We further identified C-C motif chemokine ligand 2 as a key myokine that drives MASLD, and adrenomedullin as a key hepatokine that triggers sarcopenia. ***Conclusions:*** Our findings suggest a potential bidirectional causal relationship between MASLD and sarcopenia, which may be partially mediated by C-C motif chemokine ligand 2 and adrenomedullin.

Citation of this article: Song Y, Liu Y, Jiang J, Zheng Y, Wang Z, Xie C, *et al*. Bidirectional Regulation between Metabolic Dysfunction-associated Steatotic Liver Disease and Sarcopenia via Liver-muscle Crosstalk. J Clin Transl Hepatol 2025. doi: 10.14218/JCTH.2025.00538.

Introduction

Metabolic dysfunction-associated steatotic liver disease (MASLD) represents a chronic hepatic disorder defined by ≥5% steatosis concurrent with at least one cardiometabolic risk factor.[1] With a global prevalence exceeding 30%, MASLD represents a disease spectrum ranging from simple steatosis to metabolic dysfunction-associated steatohepatitis (MASH), which may progress to advanced fibrosis, cirrhosis, and hepatocellular carcinoma, and is closely linked to obesity, diabetes, and other metabolic disorders.[2] Beyond the liver, MASLD has systemic consequences, with strong associations with cardiovascular disease, chronic kidney disease, and extrahepatic metabolic complications.[3]

Skeletal muscle, the largest insulin-sensitive organ, is central to energy balance.[4] Progressive decline in muscle mass and function, known as sarcopenia, is common in older adults and patients with chronic diseases.[5] It is reported to affect 10% to 27% of individuals aged 60 and above worldwide, substantially increasing risks of frailty, disability, and all-cause mortality.[6] Sarcopenia has been increasingly recognized as a disease rather than simply an aging phenotype, and its risk can be exacerbated by factors such as physical inactivity, inadequate nutrition, and metabolic disorders.[7]

Growing epidemiological evidence underscores a clinically significant bidirectional relationship between sarcopenia and MASLD. Several cross-sectional studies have identified that sarcopenia, independent of insulin resistance and obesity, is associated with MASLD and MASH-related advanced fibrosis.[8,9] This association carries important prognostic implications, as demonstrated by meta-analytic data showing that sarcopenic individuals face over twofold greater odds of

Keywords: Sarcopenia; Metabolic dysfunction-associated steatotic liver disease; Mendelian randomization; Liver-muscle crosstalk; C-C motif chemokine ligand 2; Adrenomedullin.

***Correspondence to:** Jian-Gao Fan, Center for Fatty Liver, Department of Gastroenterology, Xinhua Hospital Affiliated to Shanghai Jiao Tong University School of Medicine, Shanghai Key Lab of Pediatric Gastroenterology and Nutrition, Shanghai 200092, China. ORCID: https://orcid.org/0000-0002-8618-6402. Tel: +86-21-25077340, Fax: +86-21-65795173, E-mail: fanjiangao@xinhuamed.com.cn; Cen Xie, State Key Laboratory of Drug Research, Shanghai Institute of Materia Medica, Chinese Academy of Sciences, Shanghai 201203, China. ORCID: https://orcid.org/0000-0002-4574-8456. Tel/Fax: +86-21-68077984, E-mail: xiecen@simm.ac.cn.

MASLD development, alongside a 59% increased all-cause mortality risk among MASLD patients.[10] Emerging evidence also positions MASLD as an independent risk factor for sarcopenia. A multicenter prospective study demonstrated that baseline hepatic steatosis predicted incident sarcopenia even after comprehensive adjustment for age, sex, lifestyle factors, comorbidities, and metabolic confounders.[11] While these observational studies establish epidemiological associations, they cannot delineate causal directionality between sarcopenia and MASLD.

The pathogenesis of sarcopenia and MASLD demonstrates substantial mechanistic overlap, including insulin resistance, chronic low-grade inflammation, and imbalances in hormones and cytokines.[12] The liver and skeletal muscle function as endocrine organs capable of secreting a variety of proteins and metabolites, including hepatokines and myokines, that facilitate inter-organ communication.[13,14] Some of these molecules have been implicated in metabolic homeostasis. For example, muscle-derived follistatin-like protein 1 promotes the progression of MASH.[15] In contrast, increased secretion of the myokine irisin enhances lipid catabolism and effectively ameliorates hepatic injury.[16] Fetuin-A, primarily expressed and secreted by the liver, is elevated in the hepatic tissue and serum of MASLD patients and may induce insulin resistance in muscle.[17] Although certain myokines and hepatokines have been identified as key regulators in muscle atrophy, hepatic steatosis, and fibrosis, the functional roles of other secreted factors in the crosstalk between skeletal muscle and liver remain to be fully elucidated.

Currently, pharmacological interventions for coexisting MASLD and sarcopenia remain limited, partly due to a lack of adequate preclinical animal data addressing the co-occurrence and mechanistic interplay between these two conditions.[18] To address this gap, we employed an integrative approach combining human genetic analyses with complementary mouse models. First, we applied Mendelian randomization (MR) to evaluate the causal relationship between sarcopenia-related traits and MASLD risk. To experimentally dissect the liver-muscle axis, we established muscle atrophy-combined MASLD models to examine how sarcopenia influences MASLD progression. In parallel, we utilized well-established MASLD models to investigate how MASLD affects muscle function. By integrating these approaches with multi-tissue transcriptomic profiling, we aimed to construct a mechanistic framework for this inter-organ crosstalk and identify potential therapeutic strategies targeting hepatokine-myokine signaling for patients with MASLD and sarcopenia.

Methods

MR analysis

To investigate the causal relationship between sarcopenia and MASLD, we employed a two-sample MR approach. In this study, sarcopenia-related traits were defined as exposures, while MASLD was designated as the outcome. Genetic instruments for MASLD were derived from a publicly available genome-wide association study comprising 778,614 European individuals (8,434 cases and 770,180 controls).[19] Appendicular lean mass data were obtained from a genome-wide association study of 450,243 participants.[20] Furthermore, we acquired instrumental variables (IVs) associated with walking speed and leg impedance from the MRC-IEU consortium (https://gwas.mrcieu.ac.uk/). These variables involved 454,857 participants for left-leg impedance, 454,863 for right-leg impedance, and 335,349 for walking pace.

Single-nucleotide polymorphisms (SNPs) significantly associated with the exposure were selected as IVs at a genome-wide significance threshold of $p < 5 \times 10^{-8}$. The strength of the IVs was evaluated using the F-statistic, with a value greater than 10 considered indicative of a robust instrument. The F-statistic was calculated as $F = R^2 \times (N-2) / (1-R^2)$, where R^2 represents the proportion of variance in the exposure explained by the SNPs, and N is the sample size.[21] To ensure independence among the IVs, linkage disequilibrium clumping was applied with parameters set to $R^2 = 0.001$ and a window size of 10,000 kb. SNPs associated with potential confounders or the outcome were systematically removed using Phenoscanner V2. After harmonizing the exposure and outcome datasets, the remaining eligible SNPs were retained for subsequent analysis. Five MR methods were employed, with inverse variance weighting serving as the primary approach.[22] Pleiotropy was evaluated using the MR-Egger intercept test, while heterogeneity was assessed with Cochran's Q test. All analyses were conducted using the TwoSampleMR and MR-PRESSO packages in R.

Animals

Specific pathogen-free C57BL/6J mice, aged six to eight weeks, were procured from HuaFukang BioScience Company (Beijing, China) and maintained on a 12-h light cycle with ad libitum access to food and water.

For the botulinum toxin A (BTX-A)-induced sarcopenia model,[23] eight-week-old C57BL/6J mice were randomized into two groups: (i) Saline; (ii) BTX-A. Lyophilized BTX-A (Botox, Allergan Pharmaceuticals, Ireland) was reconstituted in sterile saline. Following anesthesia, the BTX-A group received intramuscular injections of BTX-A at a dose of 20 IU/kg in the right hindlimb.[24] The Saline group received equivalent volumes of saline at the same site. After two weeks, both groups were subjected to a high-fat methionine–choline-deficient diet (60 kcal% fat with 0.1% methionine and no added choline; A06071302, Research Diets, New Brunswick, USA) for three weeks.[25]

For the stelic animal model (STAM),[26] male C57BL/6J mice were randomized into two groups: (i) Ctrl; (ii) STAM. The STAM group received a single subcutaneous injection of 200 μg streptozotocin (STZ; Sigma-Aldrich, MO, USA) at postnatal day 2, followed by feeding with a high-fat diet (HFD; 60 kcal% fat; D12492, Research Diets, New Brunswick, USA) from four to seven weeks of age. Control mice were administered vehicle solution subcutaneously at postnatal day 2 and maintained on the same HFD from four weeks of age.

To establish a diet-induced MASLD model, male C57BL/6J mice (six to eight weeks old) were fed either a low-fat diet (LFD; 10 kcal% fat; D17112301R, Research Diets, New Brunswick, USA) or a Gubra-Amylin NASH (GAN) diet (40 kcal% fat, 20 kcal% fructose, and 2% cholesterol; D09100310, Research Diets, New Brunswick, USA) for 20 weeks.[25]

To establish a spontaneous obesity model, eight-week-old male leptin-deficient (*ob*/*ob*) and control (*ob*/*m*) mice, obtained from HuaFukang BioScience Company (Beijing, China), were maintained on a normal chow diet (13.5 kcal% fat; LabDiet, MO, USA) for 16 weeks.[27,28]

All animal care and experimental protocols were in accordance with the ethical guidelines of the Shanghai Institute of Materia Medica, Chinese Academy of Sciences.

Grip test

Forelimb and whole-limb grip strength were assessed using a grip strength meter (XR501, XinRuan, Shanghai, China). Mice were gently pulled horizontally by the tail after grasping a metal grid (forelimbs or all limbs).[16] Peak force from three trials was recorded and normalized to body weight.

Biochemical analysis

Serum levels of alanine aminotransferase (ALT) and aspartate aminotransferase (AST), and cellular total triglyceride (TG) levels were quantified using commercially available assay kits (Jiancheng, Nanjing, China). Hepatic total cholesterol (TC) and TG levels were measured using enzymatic colorimetric assays in accordance with the manufacturer's protocols (Jiancheng, Nanjing, China). Frozen liver tissue was homogenized in ice-cold Tris-HCl buffer containing 1% (v/v) Triton X-100. After centrifugation, the lipid-containing supernatant was analyzed.

Cell culture and treatment

All cells were maintained at 37°C in a 5% CO_2 atmosphere with saturated humidity. The C2C12 cell line (ATCC, VA, USA) was cultured in growth medium composed of high-glucose DMEM (Gibco, MA, USA), 10% fetal bovine serum (Gibco, MA, USA), and 1% penicillin–streptomycin (Meilunbio, Liaoning, China). At 90% confluence, differentiation was initiated by replacing the growth medium with differentiation medium (high-glucose DMEM supplemented with 2% horse serum and 1% penicillin–streptomycin). To induce muscle atrophy *in vitro*, myotubes were treated five days post-differentiation with 100 ng/mL recombinant murine tumor necrosis factor-alpha (TNF-α) (RP01071, ABclonal, Hubei, China) in differentiation medium for 24 h.[29]

AML12 cells (Fenghui Biotechnology, Hunan, China) were cultured in DMEM supplemented with 10% fetal bovine serum, 1% insulin–transferrin–selenium (Gibco, MA, USA), 40 ng/mL dexamethasone (MedChemExpress, Shanghai, China), and 1% penicillin–streptomycin (Meilunbio, Liaoning, China). To induce intracellular lipid accumulation, AML12 cells were treated with 0.2 mM palmitic acid (PA; Sigma-Aldrich, MO, USA) for 24 h.[30]

Following TNF-α treatment, C2C12 cells were washed with phosphate-buffered saline (PBS) and then incubated in differentiation medium. After 24 h, the conditioned medium (CM) was collected. AML12 cells were treated for 24 h with a mixture of CM and fresh intrinsic medium (3:1 ratio) along with 0.2 mM PA, followed by cellular TG quantification.

After PA treatment, AML12 cells were washed with PBS and returned to growth medium. CM was collected 24 h later. Following five days of differentiation, C2C12 myotubes were then treated for 24 h with a mixture of this CM and intrinsic medium at a 3:1 ratio.

To investigate the role of secretory factors *in vitro*, AML12 hepatocytes were treated with 200 ng/mL recombinant C-C motif chemokine ligand 2 (CCL2) protein (RP01626, ABclonal, Hubei, China), and five-day differentiated C2C12 myotubes were treated with 100 nM recombinant adrenomedullin (ADM) protein (TP09904, TenZoBio, Hubei, China) for 24 h.

ELISA

Serum and cell-CM levels of CCL2 and ADM were quantified using commercial ELISA kits (CCL2: ml037533; ADM: ml002194; both from Enzyme-Linked Biotechnology, Shanghai, China) in accordance with the manufacturer's protocols.

RNA sequencing (RNA-seq) and analysis

Total RNA was isolated from the livers and muscles of mice and subsequently subjected to high-throughput sequencing using the Illumina platform. RNA libraries were prepared using the Illumina TruSeq Stranded Total RNA Library Prep Kit (Illumina, San Diego, CA) following the manufacturer's protocol. All subsequent library processing and paired-end sequencing were conducted by Majorbio Bio-Pharm Technology (Shanghai, China) on an Illumina NovaSeq platform. Quality-filtered reads were then aligned to the murine reference genome.

Transcriptomic data were analyzed with the edgeR package to identify differentially expressed genes (DEGs). Functional annotation of DEGs was conducted using Gene Ontology (GO) and Kyoto Encyclopedia of Genes and Genomes (KEGG) pathway enrichment analyses, alongside gene set enrichment analysis, with the clusterProfiler package. Building on prior secretome profiling,[31] we identified DEGs encoding hepatokines and myokines. To systematically map liver-muscle crosstalk, we employed the NicheNetR package to analyze bulk RNA-seq data.[32]

Histological assessment

Murine muscle and liver samples were fixed in paraformaldehyde, dehydrated, and embedded in paraffin. Tissue morphology was assessed via hematoxylin and eosin (H&E) staining (Servicebio, Hubei, China), while intramuscular lipid deposition was quantified in cryosectioned samples using Oil Red O staining (Servicebio, Hubei, China). Hepatic collagen deposition was evaluated by Sirius red staining (Servicebio, Hubei, China).[30] The NAFLD activity score (NAS) was evaluated according to the histopathological characteristics observed in liver biopsy specimens, encompassing steatosis (scored 0–3), hepatocellular ballooning (scored 0–2), and lobular inflammation (scored 0–3).[33] Muscle cross-sectional area (CSA) and minimum Feret's diameter were quantified using ImageJ.[34]

Immunofluorescence staining

C2C12 myotubes were fixed with 4% paraformaldehyde for 30 min, permeabilized with 0.1% Triton X-100, and blocked with 3% bovine serum albumin in PBS for 30 min at room temperature. Subsequently, the cells were incubated overnight at 4°C with an anti-myosin heavy chain antibody (MF 20, DSHB, Iowa, USA) diluted 1:100 in blocking buffer.[35] Following primary antibody incubation, the cells were washed and then incubated with an Alexa Fluor 488-conjugated anti-mouse secondary antibody (4408S, CST, MA, USA; 1:500 dilution) and counterstained with DAPI (Beyotime, Shanghai, China). Fluorescence images were acquired using a Zeiss LSM 900 fluorescence microscope, and myotube diameter was quantified using ImageJ.

Quantitative real-time PCR

Total RNA was extracted from frozen muscle, liver, and cells using TRIzol (Yeasen Biotechnology, Shanghai, China). cDNA was synthesized with HiScript® III RT SuperMix (Vazyme, Jiangsu, China). Real-time PCR amplification was conducted using Hieff qPCR SYBR Green Master Mix (Yeasen Biotechnology, Shanghai, China) and a CFX384 system. Gene expression data were normalized to their respective housekeeping genes, using *ACTIN* for liver tissue and AML12 cells and *CYPA* for C2C12 cells. Primer sequences are detailed in Supplementary Table 1.

Statistical analysis

All statistical analyses were conducted using GraphPad Prism (GraphPad Software, CA, USA). Continuous variables are presented as mean ± standard deviation. Between-group comparisons were performed using an unpaired two-tailed Student's *t* test. The threshold for statistical significance was set at $*p < 0.05$, with more stringent levels indicated as $**p < 0.01$ and $***p < 0.001$.

Exposure	Outcome	Method	nSNP	OR (95%CI)	*p*–value	MR–Egger intercept	Int.pval
		MR Egger	588	0.88 (0.74–1.06)	0.169		
		Weighted median	588	0.95 (0.85–1.06)	0.373		
Appendicular lean mass	MASLD	IVW	588	0.91 (0.84–0.98)	0.014	0.001	0.729
		Simple mode	588	0.62 (0.41–0.94)	0.025		
		Weighted mode	588	1.21 (0.87–1.70)	0.261		
		MR Egger	29	0.09 (0.00–6.67)	0.287		
		Weighted median	29	0.25 (0.09–0.66)	0.005		
Usual walking pace	MASLD	IVW	29	0.34 (0.15–0.80)	0.013	0.013	0.553
		Simple mode	29	0.10 (0.01–0.85)	0.044		
		Weighted mode	29	0.10 (0.01–1.03)	0.063		
		MR Egger	453	0.96 (0.72–1.28)	0.778		
		Weighted median	453	0.86 (0.72–1.02)	0.078		
Impedance of leg (right)	MASLD	IVW	453	0.85 (0.76–0.95)	0.005	−0.002	0.373
		Simple mode	453	0.84 (0.50–1.42)	0.523		
		Weighted mode	453	0.92 (0.62–1.35)	0.655		
		MR Egger	460	0.89 (0.67–1.20)	0.458		
		Weighted median	460	0.86 (0.72–1.01)	0.071		
Impedance of leg (left)	MASLD	IVW	460	0.87 (0.77–0.97)	0.015	−0.001	0.822
		Simple mode	460	0.70 (0.44–1.12)	0.135		
		Weighted mode	460	0.87 (0.60–1.28)	0.492		

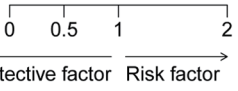

Fig. 1. Summary of the causal associations between sarcopenia-related traits and MASLD in the MR analysis. MASLD, metabolic dysfunction-associated steatotic liver disease; MR, Mendelian randomization; IVW, inverse variance weighting; SNP, single nucleotide polymorphism; OR, odds ratio.

Results

MR analysis revealed a causal relationship between sarcopenia and MASLD

Given the established clinical overlap between MASLD and sarcopenia, along with prior MR evidence indicating a causal effect of MASLD on sarcopenia risk,[36] we first investigated whether sarcopenia-related traits conversely exerted a causal influence on MASLD risk in humans. To address this, we performed two-sample MR analysis using large-scale genome-wide association studies of muscle mass, muscle function, and MASLD. Our MR analysis revealed that higher appendicular lean mass was significantly associated with reduced MASLD risk (OR 0.91, 95% CI 0.84–0.98) (Fig. 1). Walking pace, reflecting physical function, showed an even stronger protective relationship (OR 0.34, 95% CI 0.15–0.80), with consistent results observed in weighted median and simple mode analyses. Leg impedance, an indicator of muscle quality, was also inversely associated with MASLD (right leg: OR 0.85, 95% CI 0.76–0.95; left leg: OR 0.87, 95% CI 0.77–0.97). MR-Egger intercept tests indicated an absence of horizontal pleiotropy, suggesting that the IVs were not influenced by unobserved confounding factors (Fig. 1). These findings demonstrate that reduced muscle mass and impaired function increase MASLD risk, supporting a causal role of sarcopenia in MASLD pathogenesis.

BTX-A–induced muscle atrophy promoted MASLD in high-fat methionine–choline-deficient diet-fed mice

To validate this causal link experimentally, we next investigated whether sarcopenia exacerbated MASLD progression *in vivo*. We established a localized muscle atrophy model by a single intramuscular injection of BTX-A (Fig. 2A), a neurotoxin that induces muscle atrophy by blocking neuromuscular transmission.[37,38] The injection was administered into the hindlimb muscle to better recapitulate the clinical progression of sarcopenia, which affects the lower limbs more rapidly and severely than the upper limbs in humans.[39]

Administration of BTX-A resulted in a modest reduction in body weight (Fig. 2B). Compared with the saline-treated cohort, mice receiving BTX-A exhibited significantly diminished grip strength, indicative of impaired muscle function (Fig. 2C). Furthermore, BTX-A resulted in profound muscle atrophy, with significant reductions in both quadriceps femoris and gastrocnemius mass (Fig. 2D). H&E staining of muscle confirmed a decreased myofiber CSA, a diminished minimum Feret's diameter, and a leftward shift in myofiber size distribution toward smaller CSA (Fig. 2E and F).

Subsequently, we assessed whether muscle atrophy induced by BTX-A could exacerbate liver dysfunction. The ratio of liver weight to body weight was slightly higher in the BTX-A group (Fig. 2G). Serum ALT, AST, and hepatic TC levels also increased, but the differences were not statistically significant (Fig. 2H and I). In contrast, hepatic TG content was significantly increased, accompanied by marked hepatic steatosis in BTX-A-treated mice (Fig. 2I and J). Histological assessment further revealed enhanced inflammatory infiltration and fibrosis in the BTX-A group (Fig. 2J and K). RT-qPCR analysis indicated upregulation of the fatty acid transporter gene *CD36*, whereas the expression of genes involved in lipogenesis and fatty acid oxidation remained unaltered (Fig. 2L). Notably, mRNA levels of pro-inflammatory genes such as *IL1b* and *CASP1*, along with profibrotic genes, were significantly elevated in the livers of BTX-A-treated mice (Fig. 2L). Taken together, these results demonstrate that

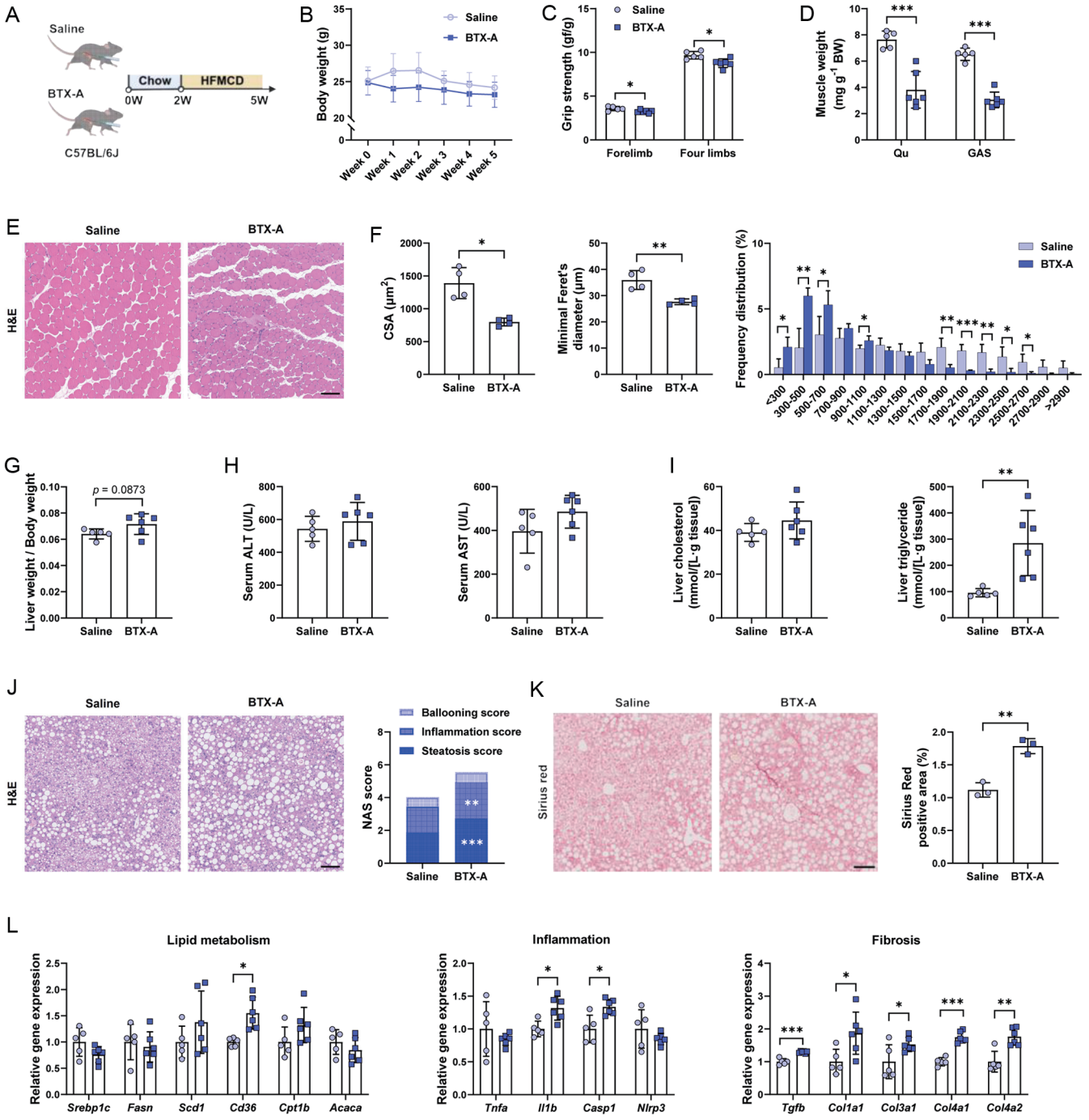

Fig. 2. The effects of BTX-A–induced muscle atrophy on MASLD. (A) Schematic of the experimental procedure of BTX-A–induced muscle atrophy and HFMCD–induced MASLD. (B) Body weight changes of the two groups (Saline, *n* = 5; BTX-A, *n* = 6). (C) Grip strength (Saline, *n* = 5; BTX-A, *n* = 6). (D) Muscle weight/body weight (Saline, *n* = 5; BTX-A, *n* = 6). (E) Representative images of H&E-stained muscle sections, scale bar = 100 μm. (F) Myofiber CSA, diameter, and myofiber CSA distribution (*n* = 4). (G) Liver weight/body weight (Saline, *n* = 5; BTX-A, *n* = 6). (H) Serum ALT and AST levels (Saline, *n* = 5; BTX-A, *n* = 6). (I) Liver cholesterol and triglyceride levels (Saline, *n* = 5; BTX-A, *n* = 6). (J) Representative liver images stained with H&E and corresponding NAS scores (*n* = 3), scale bar = 100 μm. (K) Representative Sirius red staining of liver tissue sections and quantification of the positively stained area (*n* = 3), scale bar = 100 μm. (L) Relative mRNA levels of genes related to lipid metabolism, inflammation, and fibrosis in the liver from the indicated groups (Saline, *n* = 5; BTX-A, *n* = 6). Data are presented as mean ± SD. **p* < 0.05, ***p* < 0.01, and ****p* < 0.001. MASLD, metabolic dysfunction-associated steatotic liver disease; BTX-A, botulinum toxin type A; HFMCD, high-fat methionine–choline-deficient diet; Qu, quadriceps; GAS, gastrocnemius; H&E, hematoxylin and eosin; CSA, cross-sectional area; ALT, alanine aminotransferase; AST, aspartate aminotransferase; NAS, NAFLD activity score; SREBP1c, sterol regulatory element-binding protein 1c; FASN, fatty acid synthase; SCD1, stearoyl-CoA desaturase 1; CD36, cluster of differentiation 36; CPT1b, carnitine palmitoyltransferase 1b; ACACA, acetyl-CoA carboxylase alpha; TNF-a, tumor necrosis factor alpha; IL1b, interleukin 1 beta; CASP1, caspase 1; NLRP3, NLR family pyrin domain containing 3; TGF-b, transforming growth factor beta; COL1A1, collagen type I alpha 1 chain; COL3A1, collagen type III alpha 1 chain; COL4A1, collagen type IV alpha 1 chain; COL4A2, collagen type IV alpha 2 chain.

BTX-A–induced muscle atrophy aggravated the progression of MASLD.

Coexistence of diabetic sarcopenia and MASLD in STAM mice

To further assess the association between systemic sarcopenia and MASLD, we next employed a STAM model.[26,40] In the STAM group, neonatal mice received a low, non-hepatotoxic dose of STZ via subcutaneous injection, which effectively induced pancreatic islet inflammation and dysfunction, constituting a high-risk factor for diabetic sarcopenia.[26,40] Subsequently, at four weeks of age, both the control group and the STZ-treated group were maintained on an HFD to develop MASLD (Fig. 3A).

Compared with control mice, STAM mice demonstrated a significant reduction in body weight (Fig. 3B). Notably, STAM mice exhibited severe muscle weakness, as evidenced by impaired grip strength, along with a substantial decline in muscle mass (Fig. 3C and D). Additionally, STZ administration induced a notable decrease in myofiber CSA and fiber diameter, and a shift toward smaller myofiber size distribution (Fig. 3E and F).

STAM mice exhibited significant liver dysfunction, as evidenced by a marked increase in the ratio of liver weight to body weight and elevated serum ALT and AST levels (Fig. 3G and H). Hepatic TC and TG levels were also significantly increased in STAM mice compared with controls (Fig. 3I). Histological assessment revealed severe hepatic steatosis, inflammatory infiltration, and fibrosis in STAM mice (Fig. 3J and K). Molecular analysis showed upregulated expression of *CD36* alongside downregulated lipogenic genes in the livers of STAM mice (Fig. 3L). Additionally, pro-inflammatory cytokines and profibrotic markers were significantly elevated in STAM mice relative to controls (Fig. 3L). Previous studies have shown that administration of an appropriate dose of STZ is generally sufficient to induce sarcopenia within two weeks,[34,40] whereas STZ-induced diabetes alone has a limited effect on hepatic lipid deposition, requiring a "second hit" from HFD to precipitate MASLD.[26] Together, these data demonstrate that, in the STAM model, the presence of severe sarcopenia was associated with exacerbated MASLD progression.

In summary, both the BTX-A and STAM models consistently exhibited impaired muscle function and structural atrophy, suggesting a link between sarcopenia and MASLD. In the STAM model, beyond sarcopenia, other STZ-induced systemic alterations, such as lipodystrophy and oxidative stress, may act as confounding factors that could influence the development of MASLD.[41,42] In contrast, the BTX-A model more directly illustrated the contribution of sarcopenia induced by neuromuscular inhibition.

Sarcopenia was observed in both diet-induced and genetically obese mice

Evidence from a prior MR study has indicated a causal role of MASLD in sarcopenia pathogenesis.[36] To experimentally validate this causal link, we employed a GAN diet-induced nutritional model and genetically obese leptin-deficient (*ob*/*ob*) mice (Fig. 4A and H).

Compared with *ob*/*m* controls, *ob*/*ob* mice exhibited marked obesity (Supplementary Fig. 1A and B). The *ob*/*ob* group developed severe hepatic steatosis with significantly elevated hepatic TG content (Fig. 4B and C). As expected in this genetic model,[43] no apparent fibrosis was observed (Fig. 4C). These animals also demonstrated prominent sarcopenic characteristics, including decreased grip strength, reduced muscle mass, and diminished myofiber CSA (Fig. 4D–F). Such muscular impairment was associated with ectopic lipid accumulation in skeletal muscle (Fig. 4F). Notably, all components of the NAS score were strongly inversely correlated with both muscle mass and muscle function (Fig. 4G).

To further investigate the relationship between the severity of MASLD and sarcopenia, we subjected mice to a MASH-inducing GAN diet (Fig. 4H). After 20 weeks, GAN diet-fed mice developed significant obesity (Supplementary Fig. 1C and D). Histological and biochemical assessments confirmed the onset of MASH, evidenced by pronounced hepatic steatosis, inflammation, and collagen deposition in the liver (Fig. 4I and J). Additionally, these mice displayed significant muscle weakness and atrophy compared with LFD-fed controls, as indicated by reduced grip strength, muscle mass, myofiber CSA, and increased ectopic lipid accumulation (Fig. 4K–M). Notably, all components of the NAS score and Sirius red–positive area were strongly inversely correlated with both muscle mass and muscle function, with these associations becoming more marked as MASLD severity increased (Fig. 4N).

Collectively, these results demonstrate that sarcopenia is a consistent phenotype in both dietary and genetic models of MASLD, supporting the notion that hepatic metabolic disturbances serve as a direct driver of sarcopenia progression, with the severity of muscle loss correlating with the advancement of MASLD pathology.

Transcriptomic profiling revealed sarcopenia-driven liver dysfunction via myokine signaling

Given that STZ-induced metabolic disturbances exhibit broad systemic effects due to pancreatic β-cell destruction,[26,40] whereas BTX-A–mediated muscle atrophy is more localized with minimal extra-muscular impact,[38] the BTX-A model enabled investigation of the direct impact of sarcopenia on MASLD pathogenesis. To elucidate how sarcopenia remodels liver metabolism and mediates muscle-to-liver communication, we performed RNA-seq on liver and skeletal muscle from BTX-A–treated mice and their controls.

We first identified significant transcriptomic alterations in the livers of BTX-A–induced sarcopenia models. GO analysis of upregulated DEGs revealed that sarcopenia perturbed multiple hepatic processes, particularly nutrient sensing, RNA metabolism, and transcriptional regulation (Fig. 5A). KEGG pathway analysis further demonstrated activation of mTOR signaling, insulin signaling, and PPAR signaling pathways (Fig. 5B). Conversely, GO analysis showed sarcopenia-induced downregulation of mitochondrial electron transport chain components and mitochondrial function, suggesting compromised cellular energy production and metabolic dysfunction (Fig. 5C). This was corroborated by KEGG analysis revealing broad disturbances in metabolic pathways, including oxidative phosphorylation, detoxification capacity, and cholesterol homeostasis (Fig. 5D). Additionally, gene set enrichment analysis identified significant upregulation of lipid transport pathways concurrent with suppression of lipid catabolic pathways in livers of the BTX-A group, providing a mechanistic basis for the observed exacerbation of hepatic steatosis (Fig. 5E). These findings demonstrate that sarcopenia caused broad transcriptional reprogramming in the liver, characterized by mitochondrial dysfunction and dysregulated lipid homeostasis.

Parallel RNA-seq analysis of skeletal muscle also revealed distinct changes. Pathways associated with muscle development and extracellular matrix remodeling were significantly upregulated, potentially reflecting compensatory tissue repair mechanisms in response to neuromuscular inhibition (Supplementary Fig. 2A and B). Conversely, marked down-

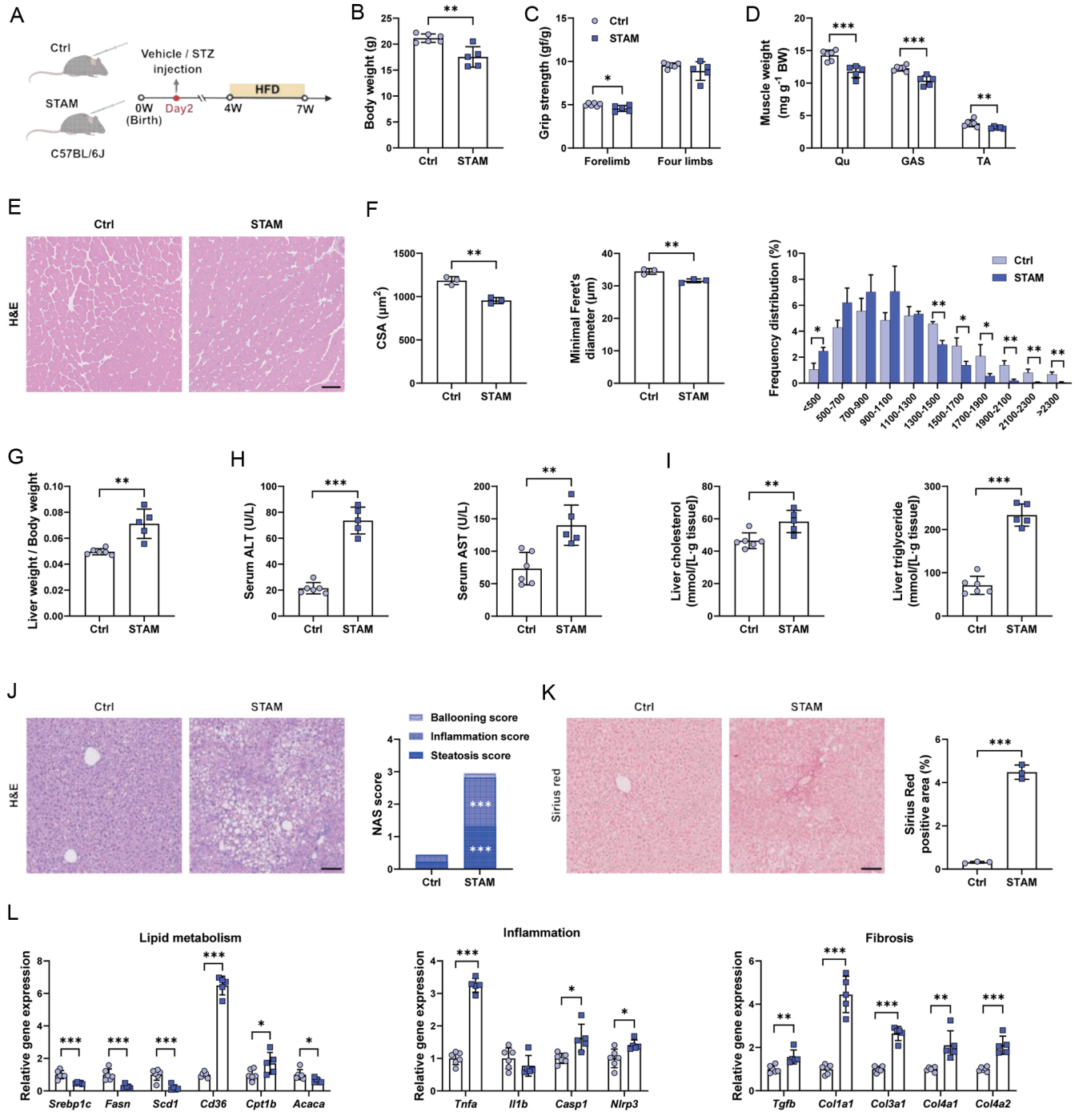

Fig. 3. Assessment of sarcopenia- and MASLD-related parameters in STAM mice. (A) Schematic of the experimental procedure of the STAM model. (B) Body weight of the two groups (Ctrl, *n* = 6; STAM, *n* = 5). (C) Grip strength (Ctrl, *n* = 6; STAM, *n* = 5). (D) Muscle weight/body weight (Ctrl, *n* = 6; STAM, *n* = 5). (E) Representative images of H&E-stained muscle sections, scale bar = 100 μm. (F) Myofiber CSA, diameter, and myofiber CSA distribution (*n* = 3). (G) Liver weight/body weight (Ctrl, *n* = 6; STAM, *n* = 5). (H) Serum ALT and AST levels (Ctrl, *n* = 6; STAM, *n* = 5). (I) Liver cholesterol and triglyceride levels (Ctrl, *n* = 6; STAM, *n* = 5). (J) Representative liver images stained with H&E and corresponding NAS scores (n = 3), scale bar = 100 μm. (K) Representative Sirius red staining of liver tissue sections and quantification of the positively stained area (*n* = 3), scale bar = 100 μm. (L) Relative mRNA levels of genes related to lipid metabolism, inflammation, and fibrosis in the liver from the indicated groups (Ctrl, *n* = 6; STAM, *n* = 5). Data are presented as mean ± SD. **p* < 0.05, ***p* < 0.01, and ****p* < 0.001. MASLD, metabolic dysfunction-associated steatotic liver disease; STAM, stelic animal model; STZ, streptozotocin; HFD, high-fat diet; Qu, quadriceps; GAS, gastrocnemius; TA, tibialis anterior; H&E, hematoxylin and eosin; CSA, cross-sectional area; ALT, alanine aminotransferase; AST, aspartate aminotransferase; NAS, NAFLD activity score; SREBP1c, sterol regulatory element-binding protein 1c; FASN, fatty acid synthase; SCD1, stearoyl-CoA desaturase 1; CD36, cluster of differentiation 36; CPT1b, carnitine palmitoyltransferase 1b; ACACA, acetyl-CoA carboxylase alpha; TNF-a, tumor necrosis factor alpha; IL1b, interleukin 1 beta; CASP1, caspase 1; NLRP3, NLR family pyrin domain containing 3; TGF-b, transforming growth factor beta; COL1A1, collagen type I alpha 1 chain; COL3A1, collagen type III alpha 1 chain; COL4A1, collagen type IV alpha 1 chain; COL4A2, collagen type IV alpha 2 chain.

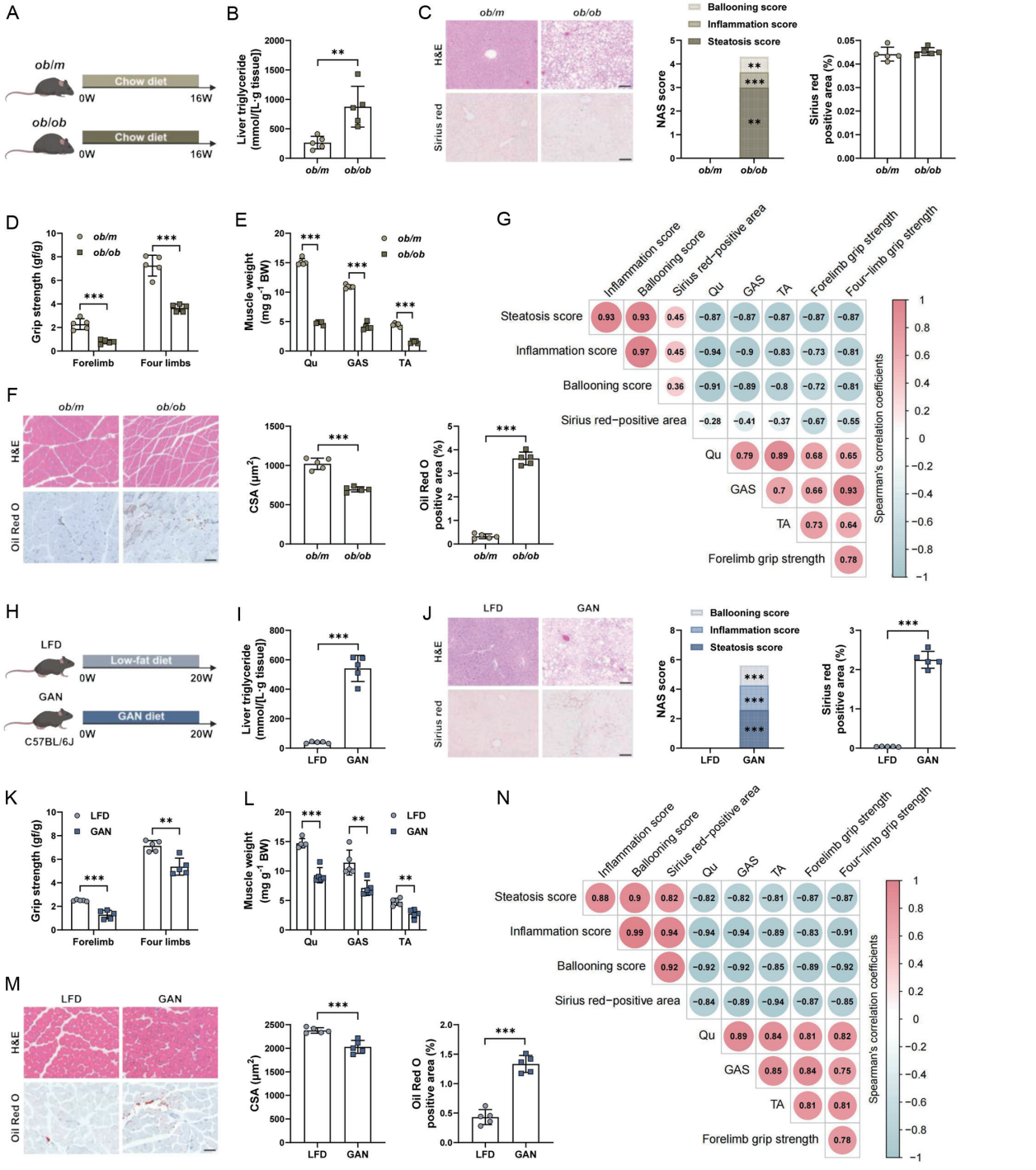

Fig. 4. The effects of MASLD on muscle mass and function. (A) Schematic of the experimental procedure of genetically induced spontaneous obesity (*ob*/*ob*) animal models. (B) Liver triglyceride levels (n = 5). (C) Representative H&E and Sirius red staining of liver sections, with the corresponding NAS score and quantification of Sirius red–positive area (n = 5), scale bar = 100 μm. (D) Grip strength (n = 5). (E) Muscle weight/body weight (n = 5). (F) Representative images of H&E and Oil Red O staining in muscle sections with quantitative analysis of myofiber CSA and lipid droplet–positive area (n = 5), scale bar = 100 μm. (G) Correlation analysis between MASLD-related indices and muscle-related parameters (n = 5). The heatmap depicts Spearman's correlation coefficients, with color intensity and circle size proportional to the correlation strength. (H) Schematic of the experimental procedure of GAN diet-induced MASLD. (I) Liver triglyceride levels (n = 5). (J) Representative H&E and Sirius red staining of liver sections, with the corresponding NAS score and quantification of Sirius red–positive area (n = 5), scale bar = 100 μm. (K) Grip strength (n = 5). (L) Muscle weight/body weight (n = 5). (M) Representative images of H&E and Oil Red O staining in muscle sections with quantitative analysis of myofiber CSA and lipid droplet–positive area (n = 5), scale bar = 100 μm. (N) Correlation analysis between MASLD-related indices and muscle-related parameters (n = 5). The heatmap depicts Spearman's correlation coefficients, with color intensity and circle size proportional to the correlation strength. Data are presented as mean ± SD. *p < 0.05, **p < 0.01, and ***p < 0.001. MASLD, metabolic dysfunction-associated steatotic liver disease; H&E, hematoxylin and eosin; NAS, NAFLD activity score; Qu, quadriceps; GAS, gastrocnemius; TA, tibialis anterior; CSA, cross-sectional area; LFD, low-fat diet; GAN, Gubra-Amylin NASH.

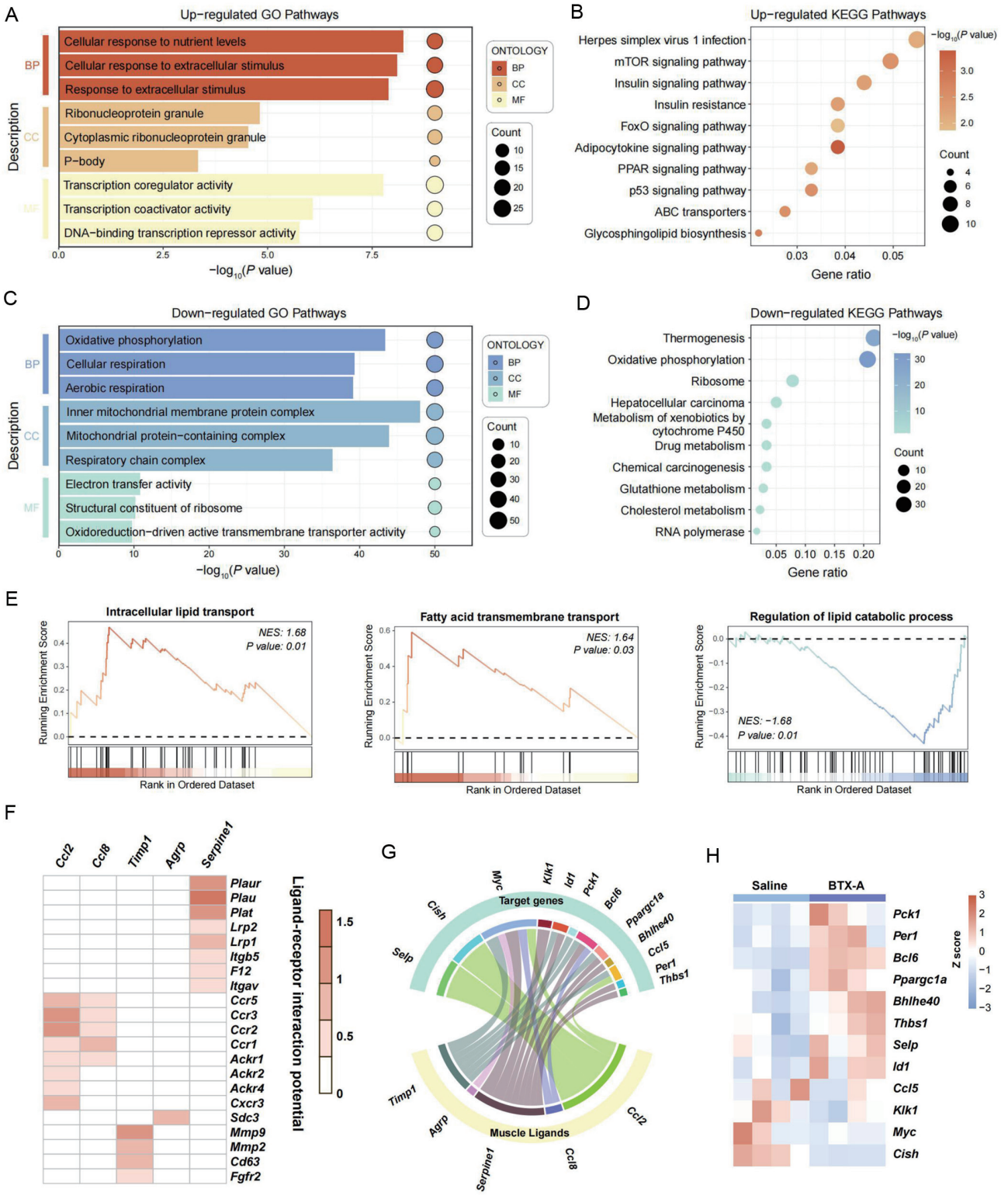

Fig. 5. Transcriptional alterations in the liver and myokine signaling during sarcopenia. (A–B) GO (A) and KEGG (B) analyses of upregulated DEGs from the liver in BTX-A vs. Saline groups. (C–D) GO (C) and KEGG (D) analyses of downregulated DEGs from the liver in BTX-A vs. Saline groups. (E) GSEA plots showing dysregulated hepatic lipid metabolic pathways in BTX-A vs. Saline groups. (F) The top five putative upregulated muscle ligands (top) and the interaction potential for the putative receptors of these ligands in the liver (right). (G) Predicted interactions between muscle ligands and their predicted hepatic target genes. (H) Expression of the target genes in the liver. DEGs, differentially expressed genes; GO, Gene Ontology; BP, biological process; CC, cellular component; MF, molecular function; KEGG, Kyoto Encyclopedia of Genes and Genomes; GSEA, gene set enrichment analysis; NES, normalized enrichment score; BTX-A, botulinum toxin type A.

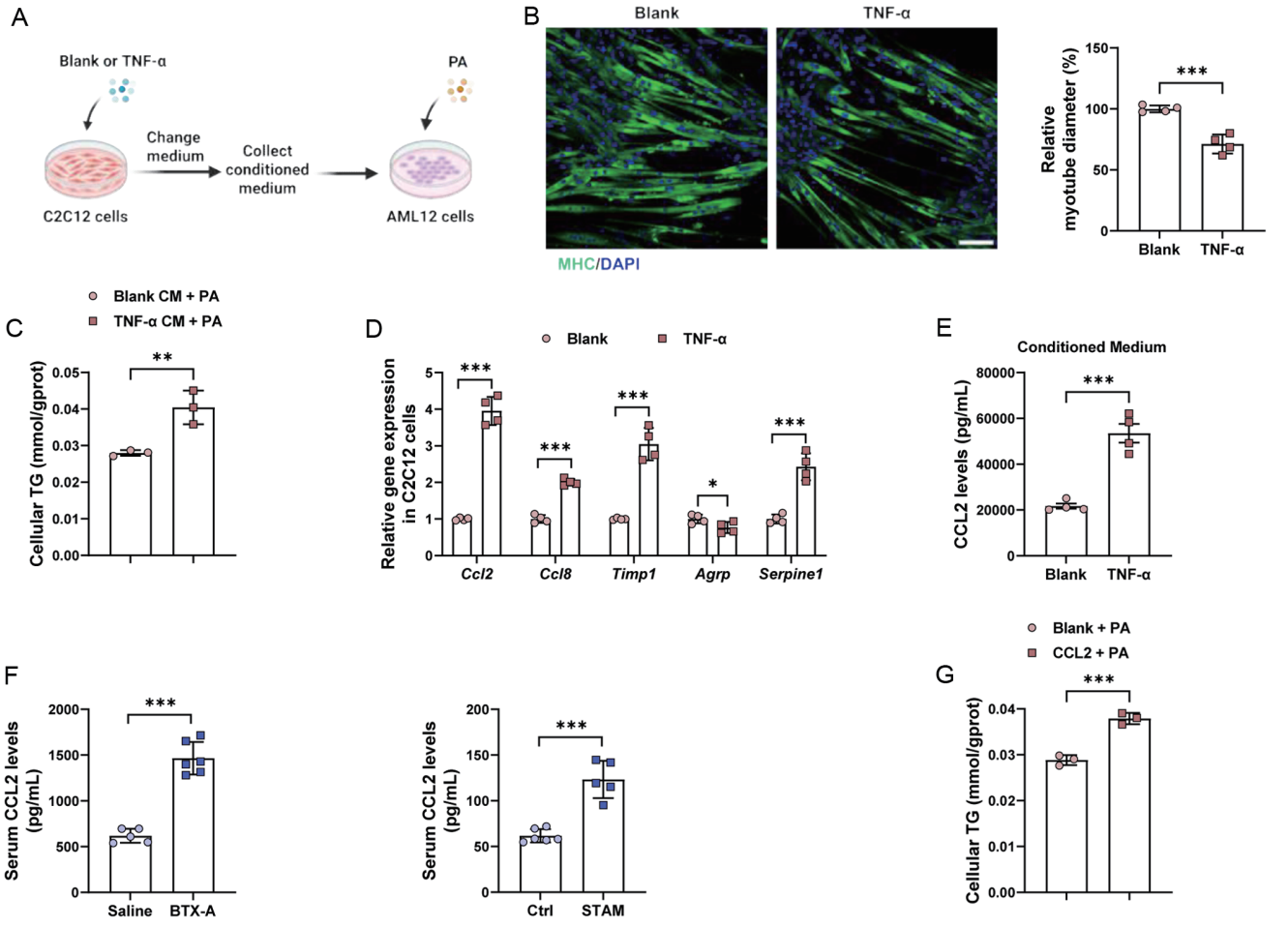

Fig. 6. Effect of muscle atrophy on hepatic lipid metabolism *in vitro*. (A) Schematic diagram of the experimental design for treating AML12 cells with CM derived from C2C12 cells stimulated with 100 ng/mL TNF-α. (B) Immunofluorescence staining of MHC and quantitative analysis of myotube diameter in TNF-α-treated C2C12 myotubes (n = 4), scale bar = 100 μm. (C) Cellular TG levels in AML12 cells following treatment with CM from C2C12 cultures (n = 3). (D) Expression levels of candidate myokine genes in C2C12 myotubes (n = 4). (E) CCL2 concentration in CM collected from C2C12 cells (n = 4). (F) Serum CCL2 levels in the indicated mouse groups (Saline, n = 5; BTX-A, n = 6; Ctrl, n = 6; STAM, n = 5). (G) Cellular TG content in AML12 cells treated with 200 ng/mL recombinant CCL2 protein (n = 3). Data are presented as mean ± SD. *p < 0.05, **p < 0.01, and ***p < 0.001. PA, palmitic acid; MHC, myosin heavy chain; DAPI, 4′,6-diamidino-2-phenylindole; TG, triglyceride; CM, conditioned medium; CCL2, C-C motif chemokine ligand 2; CCL8, C-C motif chemokine ligand 8; TIMP1, TIMP metallopeptidase inhibitor 1; AGRP, agouti-related peptide; SERPINE1, serpin family E member 1; BTX-A, botulinum toxin type A; STAM, stelic animal model.

regulation of carbohydrate metabolism and energy production pathways was observed (Supplementary Fig. 2C and D). Notably, contractile apparatus-related pathways (including myofibril, sarcomere, and calcium signaling) were substantially suppressed, consistent with the expected muscle relaxation effects of BTX-A (Supplementary Fig. 2C). These transcriptional alterations demonstrate that BTX-A induced muscle dysfunction through impaired energy metabolism and contractile dysfunction.

As the primary effector of movement and a key metabolic regulator, skeletal muscle secretes myokines that orchestrate systemic metabolic homeostasis.[13] In BTX-A–induced sarcopenia, we identified 97 upregulated and 50 downregulated myokine-encoding genes through cross-referencing muscle DEGs with a secreted protein database (Supplementary Fig. 2E).[31] To delineate muscle-liver crosstalk mechanisms, we applied NicheNet analysis using the upregulated myokines as putative ligands. This computational prediction demonstrated robust sarcopenia-associated muscle-to-liver signaling, with CCL2, CCL8, AGRP, TIMP1, and SERPINE1 emerging as the top five muscle-derived ligands exhibiting the strongest predicted regulatory activity in liver and high-affinity receptor interaction potential (Fig. 5F and Supplementary Fig. 2F). Downstream analysis identified twelve hepatic target genes regulated by the myokine signaling network (Fig. 5G and H). These results demonstrate that muscle-derived ligands in sarcopenia exerted a substantial influence on hepatic gene expression.

Collectively, these findings reveal that sarcopenia promoted hepatic steatosis through impaired mitochondrial function and disrupted lipid homeostasis and established a mechanistic link to MASLD progression via myokine-mediated interorgan communication.

CCL2 secretion induced by muscle atrophy promoted lipid accumulation in hepatocytes

To investigate whether sarcopenia directly altered hepatocyte lipid metabolism, we induced muscle atrophy *in vitro* by treating C2C12 myotubes with TNF-α, which resulted in a significant reduction in myotube diameter (Fig. 6A and B).

Following removal of TNF-α–containing medium, CM from these C2C12 cultures was collected and used to treat AML12 hepatocytes in combination with PA administration (Fig. 6A). Notably, CM from atrophic C2C12 myotubes markedly increased TG levels in AML12 cells (Fig. 6C). Based on RNA-seq data from sarcopenic mice, we identified *CCL2*, *CCL8*, *TIMP1*, *AGRP*, and *SERPINE1* as potential myokines that may mediate the effects of muscle atrophy on MASLD (Fig. 5F). Consistent with this, TNF-α–induced muscle atrophy significantly elevated the expression of *CCL2*, *CCL8*, *TIMP1*, and *SERPINE1* in C2C12 cells, with *CCL2* exhibiting the most pronounced upregulation (Fig. 6D). Increased secretion of CCL2 was further confirmed in the CM of atrophic C2C12 cells (Fig. 6E). Additionally, serum levels of CCL2 were significantly elevated in both BTX-A–treated mice and STAM mice (Fig. 6F). To functionally validate the role of CCL2, AML12 cells were treated with recombinant CCL2 protein along with PA, which resulted in a significant increase in intracellular TG accumulation (Fig. 6G). These findings demonstrate that muscle atrophy directly promoted lipid accumulation in hepatocytes and identify CCL2 as a key muscle-derived mediator linking sarcopenia to MASLD progression.

Transcriptomic profiling revealed MASLD-driven muscle dysfunction via hepatokine signaling

To investigate how MASLD contributed to skeletal muscle dysfunction and inter-organ communication, we performed RNA-seq on the liver and muscle from mice fed either an LFD or a GAN diet. This nutritional model better reflects the metabolic disturbances that initiate and drive MASLD in humans.

Significant transcriptomic alterations were first identified in skeletal muscle of MASLD models. GO analysis of upregulated DEGs indicated that MASLD affected multiple aspects of muscle biology, primarily involving immune system activation, inflammatory response, and hormone- and cytokine-related processes (Fig. 7A). Furthermore, KEGG pathway analysis demonstrated that cytokine–cytokine receptor interaction, muscle cytoskeleton, and hormone signaling pathways were upregulated, suggesting that MASLD induced muscle inflammation, remodeling, and metabolic regulation (Fig. 7B). In contrast, GO analysis revealed that the pathways most downregulated by MASLD were related to polyamine metabolism (Fig. 7C). Additionally, MASLD disrupted pathways involved in muscle secretory function and cellular polarity, potentially affecting inter-tissue communication, while KEGG analysis further demonstrated broad changes in metabolic processes, including carbohydrate, lipid, and amino acid metabolism (Fig. 7C and D). These findings demonstrate that MASLD drove inflammatory activation and metabolic dysfunction in skeletal muscle, which together may underlie the observed sarcopenic phenotype.

Parallel RNA-seq of liver tissue showed that pathways related to leukocyte activation and adhesion, collagen-containing extracellular matrix, and cytokine–cytokine receptor interaction were predominantly upregulated in MASLD livers (Supplementary Fig. 3A and B). Conversely, downregulated DEGs induced by MASLD were primarily enriched in sterol biosynthesis, protein synthesis and transport, and protease inhibitor activity (Supplementary Fig. 3C and D). These findings suggest that coordinated immune-inflammatory and fibrotic pathway activation drove hepatocyte injury in MASLD, while suppressed metabolic pathways exacerbated lipid dysregulation and protein metabolism impairment.

Emerging evidence indicates that steatotic livers exhibit altered endocrine functions compared with healthy livers, releasing differentially expressed secretory proteins (hepatokines) into circulation that may disrupt systemic metabolic homeostasis.[14] To characterize hepatokine dysregulation in MASLD, we cross-referenced hepatic DEGs with a database of secreted proteins,[31] identifying 250 upregulated and 66 downregulated hepatokine-encoding genes (Supplementary Fig. 3E). To investigate the molecular basis of liver–muscle crosstalk in MASLD, we performed NicheNet analysis using the upregulated hepatokines as putative ligands. The top five liver ligands exhibiting the highest predicted activity in MASLD were LAMA2, HBEGF, CFD, ADM, and CCL19, showing strong receptor interaction potential in muscle (Fig. 7E and Supplementary Fig. 3F). Downstream analysis identified 15 muscle target genes regulated by these hepatokines (Fig. 7F and G). These results indicate that hepatokine dysregulation in MASLD can directly reshape skeletal muscle gene expression.

Collectively, these findings establish that MASLD contributed to muscle wasting by triggering inflammatory and metabolic disruption in muscle and by altering hepatokine-mediated liver-muscle crosstalk.

ADM secretion induced by MASLD promoted myotube atrophy in vitro

To investigate the potential direct influence of MASLD on muscle atrophy, we induced hepatic lipid accumulation *in vitro* by treating AML12 hepatocytes with PA. In AML12 cells, PA exposure markedly increased intracellular TG content (Fig. 8A and B). After PA removal, CM from these lipid-laden hepatocytes was collected and applied to differentiated C2C12 myotubes (Fig. 8A). Notably, CM from PA-treated hepatocytes significantly reduced C2C12 myotube diameter, indicating a direct pro-atrophic effect on muscle cells (Fig. 8C). Based on RNA-seq data from MASLD model mice, we identified *HBEGF*, *CFD*, *ADM*, *CCL19*, and *LAMA2* as potential hepatokines that might mediate the effects of MASLD on sarcopenia (Fig. 7E). Consistent with this, PA-induced lipid accumulation significantly upregulated the expression of *CFD*, *ADM*, *CCL19*, and *LAMA2* in AML12 cells, with *ADM* showing the most pronounced increase (Fig. 8D). Enhanced secretion of ADM was further confirmed in the CM of PA-treated AML12 cells (Fig. 8E). Additionally, serum ADM levels were significantly elevated in both diet-induced MASLD mice and *ob*/*ob* mice (Fig. 8F). To functionally validate the role of ADM, C2C12 myotubes were treated with recombinant ADM protein, resulting in a significant reduction in myotube diameter (Fig. 8G). Collectively, these findings demonstrate that MASLD directly promoted myotube atrophy and that ADM secreted by steatotic hepatocytes acted as a pathogenic signal to impair muscle integrity, providing evidence for hepatokine-mediated liver–muscle crosstalk in MASLD-driven sarcopenia.

Discussion

This study provides integrated evidence that MASLD and sarcopenia are not only epidemiologically associated but also causally linked through inter-organ signaling. Using MR analysis, we demonstrated that reduced muscle mass and function increase the risk of MASLD. By employing complementary murine models, we confirmed that muscle atrophy exacerbates the progression of MASLD, while steatotic liver injury accelerates muscle dysfunction. These findings establish that sarcopenia and MASLD form a reciprocal pathogenic loop rather than independent complications of metabolic disease. Our transcriptomic and functional analyses further revealed the molecular basis of this crosstalk. Sarcopenia disrupts hepatic lipid homeostasis by upregulating fatty acid

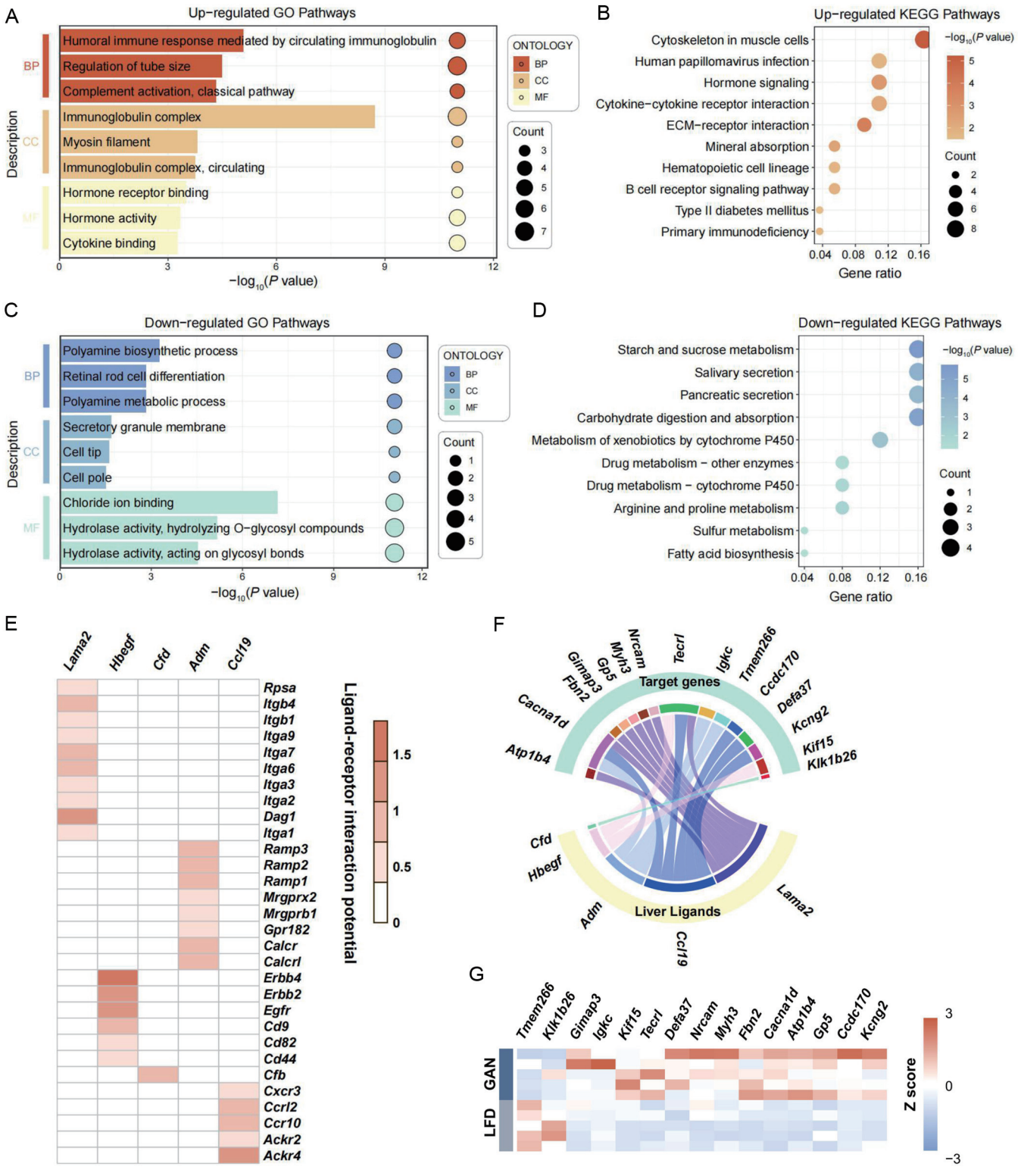

Fig. 7. Transcriptional alterations in muscle and hepatokine signaling during MASLD. (A–B) GO (A) and KEGG (B) analyses of upregulated DEGs from muscle in GAN vs. LFD groups. (C–D) GO (C) and KEGG (D) analyses of downregulated DEGs from muscle in GAN vs. LFD groups. (E) The top five putative upregulated liver ligands (top) and the interaction potential for the putative receptors of these ligands in muscle (right). (F) Predicted interactions between liver ligands and their predicted muscular target genes. (G) Expression of the target genes in muscle. MASLD, metabolic dysfunction-associated steatotic liver disease; DEGs, differentially expressed genes; GO, Gene Ontology; BP, biological process; CC, cellular component; MF, molecular function; KEGG, Kyoto Encyclopedia of Genes and Genomes; LFD, low-fat diet; GAN, Gubra-Amylin NASH.

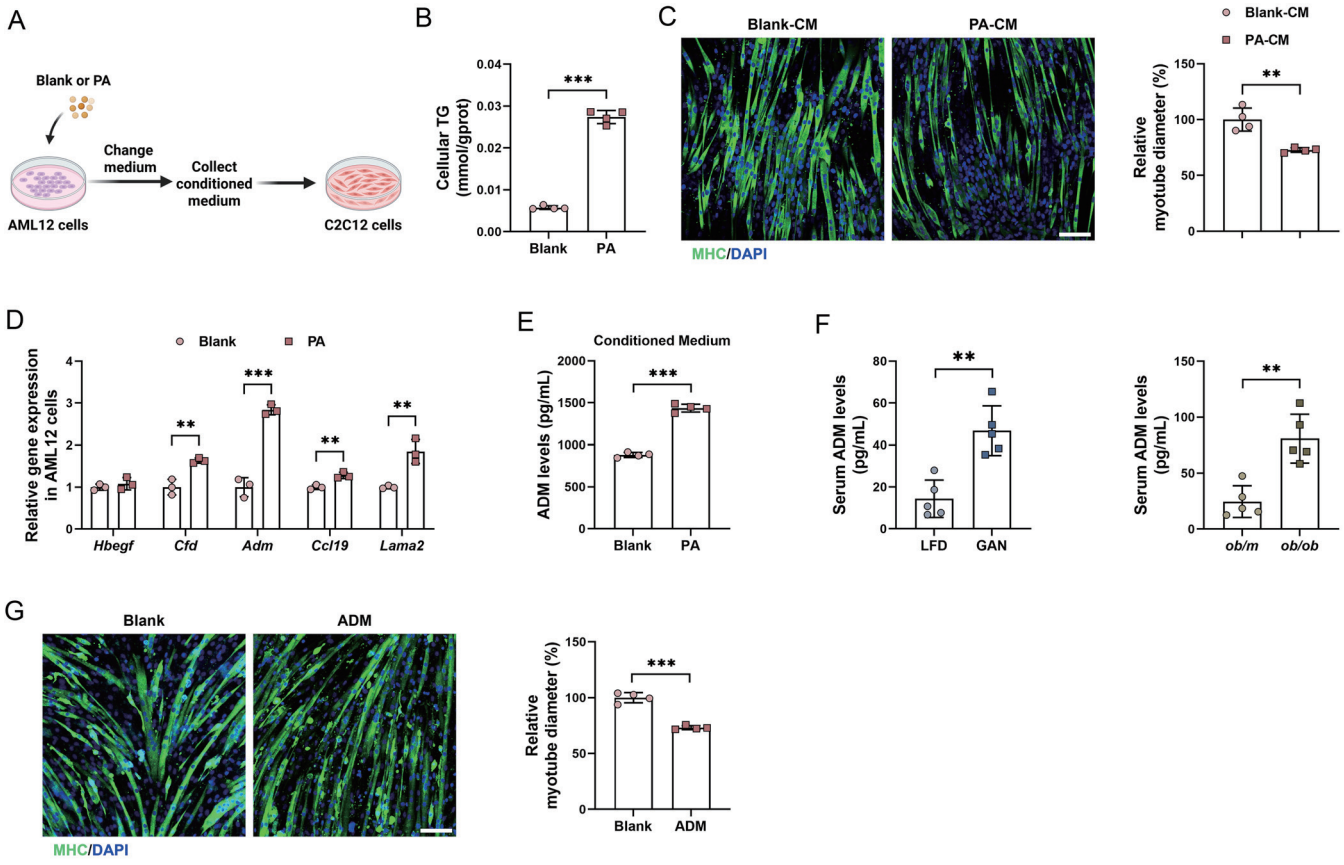

Fig. 8. Effect of hepatic lipid accumulation on myotube atrophy *in vitro*. (A) Schematic illustration of the experimental design for treating C2C12 myotubes with CM obtained from AML12 cells stimulated with 0.2 mM PA. (B) Cellular TG content in AML12 cells after treatment with 0.2 mM PA (n = 4). (C) Immunofluorescence staining of MHC and quantitative assessment of myotube diameter in C2C12 myotubes treated with CM from AML12 cell cultures (n = 4), scale bar = 100 μm. (D) Expression levels of candidate hepatokine genes in AML12 cells (n = 3). (E) ADM concentration in CM collected from AML12 cell cultures (n = 4). (F) Serum ADM levels in the indicated experimental mouse groups (n = 5). (G) Immunofluorescence staining of MHC and quantitative analysis of myotube diameter in C2C12 myotubes following treatment with 100 nM recombinant ADM protein (n = 4), scale bar = 100 μm. Data are presented as mean ± SD. *p < 0.05, **p < 0.01, and ***p < 0.001. PA, palmitic acid; MHC, myosin heavy chain; DAPI, 4′,6-diamidino-2-phenylindole; TG, triglyceride; CM, conditioned medium; ADM, adrenomedullin; HBEGF, heparin-binding EGF-like growth factor; CFD, complement factor D; CCL19, C-C motif chemokine ligand 19; LAMA2, laminin subunit alpha 2; LFD, low-fat diet; GAN, Gubra-Amylin NASH.

uptake and suppressing oxidative phosphorylation, whereas MASLD impairs muscle integrity by potentiating inflammatory responses and metabolic dysfunction. Among the secreted mediators, CCL2 emerged as a key myokine promoting hepatic lipid accumulation, while ADM was identified as a hepatokine that directly induces muscle atrophy. These results highlight a bidirectional signaling axis that links the liver and skeletal muscle and explain how MASLD and sarcopenia reinforce each other.

The causal relationship uncovered by MR analysis is in line with epidemiological evidence showing inverse associations between sarcopenia-related traits, such as appendicular lean mass, leg bioimpedance, and walking pace, and MASLD risk, suggesting potential protective effects of muscle preservation against hepatic steatosis. Currently, dietary and lifestyle modifications remain the primary therapeutic strategies for MASLD.[1] In patients with MASLD-related cirrhosis, it is particularly crucial to improve lifestyle to achieve weight reduction while preventing muscle mass loss, as sarcopenia is an independent predictor of survival, especially in patients with decompensated cirrhosis.[44]

Mechanistically, both BTX-A-treated mice and STAM mice exhibited increased hepatic lipid accumulation, partly through increased *CD36* expression, implicating enhanced fatty acid uptake as a driver of steatosis. This aligns with studies showing increased CD36 localization on hepatocyte membranes in MASH patients, where CD36 palmitoylation promotes free fatty acid uptake and exacerbates intracellular lipid deposition.[45] Additionally, our RNA-seq data revealed an upregulation of pathways associated with hepatic lipid transport in the BTX-A group. Moreover, mitochondrial dysfunction likely further disrupts liver lipid metabolic homeostasis and promotes MASH progression.[46]

In this study, we identified CCL2 as a critical myokine that mediates the pathogenic crosstalk between skeletal muscle and liver. As a key chemokine, CCL2 is known for its role in immune cell chemotaxis and inflammatory responses.[47] Recent studies have shown that CCL2 expression is upregulated in specific subpopulations of muscle stem cells within senescent human skeletal muscle, as well as in various cell types in the muscle fiber microenvironment, where it contributes to disrupted immune homeostasis.[48] Our data suggest that muscle-derived CCL2 may enter the circulation and exert effects on the liver. Previous studies have demonstrated that inhibition of CCL2 during chronic liver injury attenuates steatohepatitis by reducing hepatic monocyte and macrophage infiltration.[49]

This study demonstrates that obesity induces not only

hepatic steatosis but also profound sarcopenic alterations in mice, including diminished grip strength, reduced myofiber CSA, and increased intramuscular lipid deposition. These findings are consistent with clinical observations of the high prevalence of sarcopenic obesity in MASLD patients.[50] Notably, the pathological significance of myosteatosis extends beyond muscle dysfunction, as emerging evidence indicates that it independently predicts MASH development, fibrosis progression, and adverse outcomes in cirrhosis, underscoring the pathological importance of altered muscle lipid metabolism.[51,52]

Our transcriptomic analysis demonstrated concurrent activation of inflammatory pathways in both liver and skeletal muscle under MASLD conditions. In the obese state, numerous cytokines released by immune cells and adipocytes, such as interleukin-6, C-reactive protein, and TNF-α, induce chronic low-grade inflammation.[53] The progression of MASLD is markedly accelerated through a multistage inflammatory cascade, comprising immune cell activation, proinflammatory cytokine release, and establishment of chronic inflammation.[54] This inflammatory milieu disrupts insulin and IGF-1 signaling, promotes endoplasmic reticulum stress and mitochondrial dysfunction in skeletal muscle, and collectively drives insulin resistance, protein metabolism imbalance, and muscle atrophy.[7]

In the reverse direction, ADM was identified as a critical hepatokine linking steatotic liver to muscle atrophy. As a peptide hormone, ADM is known primarily for its roles in regulating vascular tone, vascular remodeling, and endothelial barrier function and integrity.[55] A recent study highlighted its involvement in type 2 diabetes, reporting elevated plasma levels of ADM in both obese humans and mice.[56] Specifically, ADM was shown to activate protein tyrosine phosphatase 1B, which inhibits phosphorylation of the insulin receptor in vascular endothelial cells, thereby impairing insulin signaling.[56] Treatment of mice with an ADM mimetic recapitulated the effects of obesity, inducing both endothelial and systemic insulin resistance.[56]

Building upon the direct atrophic effects of ADM on myocytes in our study, an intriguing question arises regarding its potential interplay with muscle-derived CCL2. We hypothesize that ADM and CCL2 may reinforce each other by mutually exacerbating insulin resistance and chronic inflammation. On one hand, ADM-mediated insulin resistance may diminish the anti-inflammatory effects of insulin, thereby potentially augmenting CCL2 expression.[56,57] Conversely, elevated levels of CCL2 may exacerbate hepatic inflammation,[49] which in turn can further enhance the secretion of hepatic ADM via cytokines such as TNF-α.[58,59] The subsequently increased ADM may then circulate back to muscle, worsening insulin resistance and muscle atrophy. Therefore, beyond their direct roles, ADM and CCL2 likely form a self-amplifying axis that disrupts muscle-liver crosstalk, a mechanism that warrants further investigation.

Several limitations warrant attention. The MR analysis was conducted exclusively in European populations, potentially limiting the extrapolation of our findings to other ethnic groups. Regarding animal models, while BTX-A-induced muscle atrophy replicates core sarcopenia features, it does not fully emulate the chronic and systemic progression of age-related muscle decline observed in humans.[39] Similarly, the STAM model induces insulin-deficient diabetes rather than the insulin-resistant state typically observed in MASLD-associated sarcopenia patients.[7,60] It is necessary to design longitudinal studies to clarify the temporal relationship between the onset of sarcopenia and MASLD, especially in STAM mice, GAN diet-induced MASLD mice, and *ob*/*ob* mice. While the roles of CCL2 and ADM have been established *in vitro*, their *in vivo* functions and the potential interplay between their downstream signaling pathways warrant further investigation. Furthermore, the clinical relevance and translational potential of these mechanisms identified in murine models to human pathophysiology remain to be elucidated.

Conclusions

Our study reveals a potential bidirectional causal relationship between MASLD and sarcopenia through liver-muscle crosstalk. By integrating MR analysis, complementary mouse models, and multi-tissue transcriptomics, we identified CCL2 and ADM as putative mediators of this inter-organ communication. These findings underscore the importance of viewing MASLD and sarcopenia as interconnected disorders, and targeting the hepatokine-myokine axis may break the vicious cycle that sustains both diseases. Future studies are needed to clarify the temporal sequence of sarcopenia onset and MASLD progression, and to further elucidate the downstream signaling pathways involving CCL2 and ADM.

Acknowledgments

We thank the MRC-IEU consortium for providing their invaluable genome-wide association study data, which are essential for our research.

Funding

This study was supported by grants from the Noncommunicable Chronic Diseases–National Science and Technology Major Project (Grant No. 2023ZD0508700 to JGF), the National Key Research and Development Program of China (Grant No. 2021YFA1301200 to CX), the National Natural Science Foundation of China (Grant No. 82222071 to CX, and 82170593 and 82470600 to JGF), and the Strategic Priority Research Program of the Chinese Academy of Sciences (Grant No. XDB0830402 to CX).

Conflict of interest

JGF has been an Associate Editor of the *Journal of Clinical and Translational Hepatology* since 2013. The other authors have no conflict of interests related to this publication.

Author contributions

Study design, study supervision (JGF, CX), experiment performance (YS, YL, JJ, YZ), preparation of materials (YS, JJ, YZ, YL), data analysis (YS), technical support (YZ, ZW), and writing of the manuscript (YS, CX). All authors have made significant contributions to this study and have approved the final manuscript.

Ethical statement

All animal handling and experimental protocols received approval from the Bioethics Committee at the Shanghai Institute of Materia Medica, Chinese Academy of Sciences (Approval No. 2022-08-XC-69), in compliance with the ARRIVE guidelines. All animals were provided with humane care.

Data sharing statement

The data utilized and examined in this study can be accessed upon reasonable request from the corresponding author.

References

[1] Fan JG, Xu XY, Yang RX, Nan YM, Wei L, Jia JD, *et al*. Guideline for the Prevention and Treatment of Metabolic Dysfunction-associated Fatty Liver Disease (Version 2024). J Clin Transl Hepatol 2024;12(11):955–974. doi:10.14218/JCTH.2024.00311, PMID:39544247.

[2] Younossi ZM, Golabi P, Paik JM, Henry A, Van Dongen C, Henry L. The global epidemiology of nonalcoholic fatty liver disease (NAFLD) and nonalcoholic steatohepatitis (NASH): a systematic review. Hepatology 2023;77(4):1335–1347. doi:10.1097/HEP.0000000000000004, PMID:36626630.

[3] Miao L, Targher G, Byrne CD, Cao YY, Zheng MH. Current status and future trends of the global burden of MASLD. Trends Endocrinol Metab 2024;35(8):697–707. doi:10.1016/j.tem.2024.02.007, PMID:38429161.

[4] Boccardi V. Sarcopenia: A dive into metabolism to promote a multimodal, preventive, and regenerative approach. Mech Ageing Dev 2024;219:111941. doi:10.1016/j.mad.2024.111941, PMID:38750969.

[5] Yuan S, Larsson SC. Epidemiology of sarcopenia: Prevalence, risk factors, and consequences. Metabolism 2023;144:155533. doi:10.1016/j.metabol.2023.155533, PMID:36907247.

[6] Petermann-Rocha F, Balntzi V, Gray SR, Lara J, Ho FK, Pell JP, *et al*. Global prevalence of sarcopenia and severe sarcopenia: a systematic review and meta-analysis. J Cachexia Sarcopenia Muscle 2022;13(1):86–99. doi:10.1002/jcsm.12783, PMID:34816624.

[7] Prado CM, Batsis JA, Donini LM, Gonzalez MC, Siervo M. Sarcopenic obesity in older adults: a clinical overview. Nat Rev Endocrinol 2024;20(5):261–277. doi:10.1038/s41574-023-00943-z, PMID:38321142.

[8] Lee YH, Jung KS, Kim SU, Yoon HJ, Yun YJ, Lee BW, *et al*. Sarcopaenia is associated with NAFLD independently of obesity and insulin resistance: Nationwide surveys (KNHANES 2008-2011). J Hepatol 2015;63(2):486–493. doi:10.1016/j.jhep.2015.02.051, PMID:25772036.

[9] Koo BK, Kim D, Joo SK, Kim JH, Chang MS, Kim BG, *et al*. Sarcopenia is an independent risk factor for non-alcoholic steatohepatitis and significant fibrosis. J Hepatol 2017;66(1):123–131. doi:10.1016/j.jhep.2016.08.019, PMID:27599824.

[10] Li X, He J, Sun Q. The prevalence and effects of sarcopenia in patients with metabolic dysfunction-associated steatotic liver disease (MASLD): A systematic review and meta-analysis. Clin Nutr 2024;43(9):2005–2016. doi:10.1016/j.clnu.2024.07.006, PMID:39053329.

[11] Roh E, Hwang SY, Yoo HJ, Baik SH, Lee JH, Son SJ, *et al*. Impact of nonalcoholic fatty liver disease on the risk of sarcopenia: a nationwide multicenter prospective study. Hepatol Int 2022;16(3):545–554. doi:10.1007/s12072-021-10258-8, PMID:34780030.

[12] Kuchay MS, Martínez-Montoro JI, Kaur P, Fernández-García JC, Ramos-Molina B. Non-alcoholic fatty liver disease-related fibrosis and sarcopenia: An altered liver-muscle crosstalk leading to increased mortality risk. Ageing Res Rev 2022;80:101696. doi:10.1016/j.arr.2022.101696, PMID:35843589.

[13] Chen ZT, Weng ZX, Lin JD, Meng ZX. Myokines: metabolic regulation in obesity and type 2 diabetes. Life Metab 2024;3(3):loae006. doi:10.1093/lifemeta/loae006, PMID:39872377.

[14] Stefan N, Schick F, Birkenfeld AL, Häring HU, White MF. The role of hepatokines in NAFLD. Cell Metab 2023;35(2):236–252. doi:10.1016/j.cmet.2023.01.006, PMID:36754018.

[15] Guo S, Feng Y, Zhu X, Zhang X, Wang H, Wang R, *et al*. Metabolic crosstalk between skeletal muscle cells and liver through IRF4-FSTL1 in nonalcoholic steatohepatitis. Nat Commun 2023;14(1):6047. doi:10.1038/s41467-023-41832-3, PMID:37770480.

[16] Wang C, Liu K, Ji J, Ma W, Zhang H, Wang K, *et al*. Liu-Jun-Zi decoction alleviates metabolic dysfunction-associated steatohepatitis by modulating myogenic irisin mediated skeletal muscle-liver crosstalk. Phytomedicine 2025;148:157218. doi:10.1016/j.phymed.2025.157218, PMID:40992068.

[17] Marjot T, Armstrong MJ, Stine JG. Skeletal muscle and MASLD: Mechanistic and clinical insights. Hepatol Commun 2025;9(6):e0711. doi:10.1097/HC9.0000000000000711, PMID:40408301.

[18] Liu CH, Zeng QM, Kim W, Kim SU, Younossi ZM, Targher G, *et al*. Sarcopenia and MASLD: novel insights and the future. Nat Rev Endocrinol 2025. doi:10.1038/s41574-025-01197-7, PMID:41193695.

[19] Ghodsian N, Abner E, Emdin CA, Gobeil É, Taba N, Haas ME, *et al*. Electronic health record-based genome-wide meta-analysis provides insights on the genetic architecture of non-alcoholic fatty liver disease. Cell Rep Med 2021;2(11):100437. doi:10.1016/j.xcrm.2021.100437, PMID:34841290.

[20] Pei YF, Liu YZ, Yang XL, Zhang H, Feng GJ, Wei XT, *et al*. The genetic architecture of appendicular lean mass characterized by association analysis in the UK Biobank study. Commun Biol 2020;3(1):608. doi:10.1038/s42003-020-01334-0, PMID:33097823.

[21] Li J, Wang J, Yang M, Wang G, Xu P. The relationship between major depression and delirium: A two-sample Mendelian randomization analysis. J Affect Disord 2023;338:69–73. doi:10.1016/j.jad.2023.05.046, PMID:37244544.

[22] Davies NM, Holmes MV, Davey Smith G. Reading Mendelian randomisation studies: a guide, glossary, and checklist for clinicians. BMJ 2018;362:k601. doi:10.1136/bmj.k601, PMID:30002074.

[23] Stone AV, Ma J, Callahan MF, Smith BP, Garrett JP, Smith TL, *et al*. Dose- and volume dependent-response to intramuscular injection of botulinum neurotoxin-A optimizes muscle force decrement in mice. J Orthop Res 2011;29(11):1764–1770. doi:10.1002/jor.21434, PMID:21491479.

[24] Babuccu B, Babuccu O, Yurdakan G, Ankarali H. The effect of the Botulinum toxin-A on craniofacial development: an experimental study. Ann Plast Surg 2009;63(4):449–456. doi:10.1097/SAP.0b013e31818d4559, PMID:19745716.

[25] Jiang J, Gao Y, Wang J, Huang Y, Yang R, Zhang Y, *et al*. Hepatic sphingomyelin phosphodiesterase 3 promotes steatohepatitis by disrupting membrane sphingolipid metabolism. Cell Metab 2025;37(5):1119–1136.e13. doi:10.1016/j.cmet.2025.01.016, PMID:40015281.

[26] Saito T, Muramatsu M, Ishii Y, Saigo Y, Konuma T, Toriniwa Y, *et al*. Pathophysiological analysis of the progression of hepatic lesions in STAM mice. Physiol Res 2017;66(5):791–799. doi:10.33549/physiolres.933592, PMID:28730823.

[27] Xu H, Wang J, Liu Y, Wang Y, Zhong X, Li C, *et al*. Development of a simultaneous quantification method for the gut microbiota-derived core nutrient metabolome in mice and its application in studying host-microbiota interaction. Anal Chim Acta 2023;1251:341039. doi:10.1016/j.aca.2023.341039, PMID:36925303.

[28] López-Herrador S, Torres-Rusillo S, González-García P, Jiménez-Sánchez L, Corral-Sarasa J, Bakkali M, *et al*. β-Resorcylic acid prevents MASLD in ob/ob mice by modulating lipid metabolism and inflammation in the liver. Pharmacol Res 2025;219:107906. doi:10.1016/j.phrs.2025.107906, PMID:40789566.

[29] Li J, Chan MC, Yu Y, Bei Y, Chen P, Zhou Q, *et al*. miR-29b contributes to multiple types of muscle atrophy. Nat Commun 2017;8:15201. doi:10.1038/ncomms15201, PMID:28541289.

[30] Hu S, Liang X, Qin Y, Li Y, Liu Y, Liu C, *et al*. Alnustone Ameliorates Metabolic Dysfunction-Associated Steatotic Liver Disease by Facilitating Mitochondrial Fatty Acid β-Oxidation via Targeting Calmodulin. Adv Sci (Weinh) 2025;12(31):e11984. doi:10.1002/advs.202411984, PMID:40470949.

[31] Xiong X, Kuang H, Ansari S, Liu T, Gong J, Wang S, *et al*. Landscape of Intercellular Crosstalk in Healthy and NASH Liver Revealed by Single-Cell Secretome Gene Analysis. Mol Cell 2019;75(3):644–660.e5. doi:10.1016/j.molcel.2019.07.028, PMID:31398325.

[32] Feng Y, Cui Z, Lu X, Gong H, Liu X, Wang H, *et al*. Transcriptomics Dissection of Calorie Restriction and Exercise Training in Brown Adipose Tissue and Skeletal Muscle. Nutrients 2023;15(4):1047. doi:10.3390/nu15041047, PMID:36839405.

[33] Kleiner DE, Brunt EM, Van Natta M, Behling C, Contos MJ, Cummings OW, *et al*. Design and validation of a histological scoring system for nonalcoholic fatty liver disease. Hepatology 2005;41(6):1313–1321. doi:10.1002/hep.20701, PMID:15915461.

[34] Fujimaki S, Matsumoto T, Muramatsu M, Nagahisa H, Horii N, Seko D, *et al*. The endothelial Dll4-muscular Notch2 axis regulates skeletal muscle mass. Nat Metab 2022;4(2):180–189. doi:10.1038/s42255-022-00533-9, PMID:35228746.

[35] Zhang R, Shen Q, Wang Y, Deng X, Fan J, Gu X, *et al*. Corylifol A ameliorates muscle atrophy by inhibiting TAOK1/p38-MAPK/FoxO3 pathway in cancer cachexia. J Cachexia Sarcopenia Muscle 2023;14(5):2098–2113. doi:10.1002/jcsm.13288, PMID:37439183.

[36] Yuan J, Zhang J, Luo Q, Peng L. Effects of nonalcoholic fatty liver disease on sarcopenia: evidence from genetic methods. Sci Rep 2024;14(1):2709. doi:10.1038/s41598-024-53112-1, PMID:38302636.

[37] Multani I, Manji J, Tang MJ, Herzog W, Howard JJ, Graham HK. Sarcopenia, Cerebral Palsy, and Botulinum Toxin Type A. JBJS Rev 2019;7(8):e4. doi:10.2106/JBJS.RVW.18.00153, PMID:31415277.

[38] Moritz MS, Tepp WH, Inzalaco HN, Johnson EA, Pellett S. Comparative functional analysis of mice after local injection with botulinum neurotoxin A1, A2, A6, and B1 by catwalk analysis. Toxicon 2019;167:20–28. doi:10.1016/j.toxicon.2019.06.004, PMID:31181297.

[39] Sayer AA, Cooper R, Arai H, Cawthon PM, Ntsama Essomba MJ, Fielding RA, *et al*. Sarcopenia. Nat Rev Dis Primers 2024;10(1):68. doi:10.1038/s41572-024-00550-w, PMID:39300120.

[40] Hirata Y, Nomura K, Senga Y, Okada Y, Kobayashi K, Okamoto S, *et al*. Hyperglycemia induces skeletal muscle atrophy via a WWP1/KLF15 axis. JCI Insight 2019;4(4):124952. doi:10.1172/jci.insight.124952, PMID:30830866.

[41] Carpéné C, Stiliyanov Atanasov K, Les F, Mercader Barcelo J. Hyperglycemia and reduced adiposity of streptozotocin-induced diabetic mice are not alleviated by oral benzylamine supplementation. World J Diabetes 2022;13(9):752–764. doi:10.4239/wjd.v13.i9.752, PMID:36188146.

[42] Volpe CMO, Villar-Delfino PH, Dos Anjos PMF, Nogueira-Machado JA. Cellular death, reactive oxygen species (ROS) and diabetic complications. Cell Death Dis 2018;9(2):119. doi:10.1038/s41419-017-0135-z, PMID:29371661.

[43] Leclercq IA, Farrell GC, Schriemer R, Robertson GR. Leptin is essential for the hepatic fibrogenic response to chronic liver injury. J Hepatol 2002;37(2):206–213. doi:10.1016/s0168-8278(02)00102-2, PMID:12127425.

[44] Mallet M, Silaghi CA, Sultanik P, Conti F, Rudler M, Ratziu V, *et al*. Current challenges and future perspectives in treating patients with NAFLD-related cirrhosis. Hepatology 2024;80(5):1270–1290. doi:10.1097/HEP.0000000000000456, PMID:37183906.

[45] Zhao L, Zhang C, Luo X, Wang P, Zhou W, Zhong S, *et al*. CD36 palmitoylation disrupts free fatty acid metabolism and promotes tissue inflammation in non-alcoholic steatohepatitis. J Hepatol 2018;69(3):705–717. doi:10.1016/j.jhep.2018.04.006, PMID:29705240.

[46] Radosavljevic T, Brankovic M, Samardzic J, Djuretić J, Vukicevic D, Vucevic D, *et al*. Altered Mitochondrial Function in MASLD: Key Features and Promising Therapeutic Approaches. Antioxidants (Basel) 2024;13(8):906. doi:10.3390/antiox13080906, PMID:39199152.

[47] Dhengle S, Maharana KC, Meenakshi S, Singh S. Mechanistic Insights into the Role of MCP-1 in Diverse Liver Pathological Conditions: A Recent Update. Curr Pharm Des 2025;31(15):1167–1179. doi:10.2174/0113816128332969241120030733, PMID:39779567.

[48] Kedlian VR, Wang Y, Liu T, Chen X, Bolt L, Tudor C, *et al*. Human skeletal muscle aging atlas. Nat Aging 2024;4(5):727–744. doi:10.1038/s43587-

024-00613-3, PMID:38622407.
[49] Baeck C, Wehr A, Karlmark KR, Heymann F, Vucur M, Gassler N, *et al*. Pharmacological inhibition of the chemokine CCL2 (MCP-1) diminishes liver macrophage infiltration and steatohepatitis in chronic hepatic injury. Gut 2012;61(3):416–426. doi:10.1136/gutjnl-2011-300304, PMID:21813474.
[50] Chun HS, Lee M, Lee HA, Lee S, Kim S, Jung YJ, *et al*. Risk Stratification for Sarcopenic Obesity in Subjects With Nonalcoholic Fatty Liver Disease. Clin Gastroenterol Hepatol 2023;21(9):2298–2307.e18. doi:10.1016/j.cgh.2022.11.031, PMID:36462755.
[51] Hsieh YC, Joo SK, Koo BK, Lin HC, Lee DH, Chang MS, *et al*. Myosteatosis, but not Sarcopenia, Predisposes NAFLD Subjects to Early Steatohepatitis and Fibrosis Progression. Clin Gastroenterol Hepatol 2023;21(2):388–397.e10. doi:10.1016/j.cgh.2022.01.020, PMID:35101634.
[52] Di Cola S, D'Amico G, Caraceni P, Schepis F, Loredana S, Lampertico P, *et al*. Myosteatosis is closely associated with sarcopenia and significantly worse outcomes in patients with cirrhosis. J Hepatol 2024;81(4):641–650. doi:10.1016/j.jhep.2024.05.020, PMID:38782120.
[53] Han JW, Kim DI, Nam HC, Chang UI, Yang JM, Song DS. Association between serum tumor necrosis factor-α and sarcopenia in liver cirrhosis. Clin Mol Hepatol 2022;28(2):219–231. doi:10.3350/cmh.2021.0082, PMID:34281295.
[54] Mladenić K, Lenartić M, Marinović S, Polić B, Wensveen FM. The "Domino effect" in MASLD: The inflammatory cascade of steatohepatitis. Eur J Immunol 2024;54(4):e2149641. doi:10.1002/eji.202149641, PMID:38314819.
[55] Bálint L, Nelson-Maney NP, Tian Y, Serafin SD, Caron KM. Clinical Potential of Adrenomedullin Signaling in the Cardiovascular System. Circ Res 2023;132(9):1185–1202. doi:10.1161/CIRCRESAHA.123.321673, PMID:37104556.
[56] Cho H, Lai CC, Bonnavion R, Alnouri MW, Wang S, Roquid KA, *et al*. Endothelial insulin resistance induced by adrenomedullin mediates obesity-associated diabetes. Science 2025;387(6734):674–682. doi:10.1126/science.adr4731, PMID:39913566.
[57] Aljada A, Ghanim H, Saadeh R, Dandona P. Insulin inhibits NFkappaB and MCP-1 expression in human aortic endothelial cells. J Clin Endocrinol Metab 2001;86(1):450–453. doi:10.1210/jcem.86.1.7278, PMID:11232040.
[58] Li Y, Totsune K, Takeda K, Furuyama K, Shibahara S, Takahashi K. Differential expression of adrenomedullin and resistin in 3T3-L1 adipocytes treated with tumor necrosis factor-alpha. Eur J Endocrinol 2003;149(3):231–238. doi:10.1530/eje.0.1490231, PMID:12943526.
[59] Nikitenko LL, Fox SB, Kehoe S, Rees MC, Bicknell R. Adrenomedullin and tumour angiogenesis. Br J Cancer 2006;94(1):1–7. doi:10.1038/sj.bjc.6602832, PMID:16251875.
[60] Farrell G, Schattenberg JM, Leclercq I, Yeh MM, Goldin R, Teoh N, *et al*. Mouse Models of Nonalcoholic Steatohepatitis: Toward Optimization of Their Relevance to Human Nonalcoholic Steatohepatitis. Hepatology 2019;69(5):2241–2257. doi:10.1002/hep.30333, PMID:30372785.